JOURNAL OF INFORMATION SCIENCE AND ENGINEERING 33, 1611-1627 (2017)
DOI: 10.6688/JISE.2017.33.6.14

A Novel Fast GLM Approach for Retinal Vascular Segmentation and Denoising

KHAN BAHADAR KHAN[1,*], AMIR A. KHALIQ[1] AND MUHAMMAD SHAHID[2]
[1]*Department of Electronic Engineering*
International Islamic University
Islamabad 44000, Pakistan
[2]*Department of Electrical Engineering*
Capital University of Science and Technology
Islamabad 44000, Pakistan
E-mail: {Bahadar.phdee46; m.amir}@iiu.edu.pk; shahid.eyecom@gmail.com

Precise retinal vessels localization is an important and challenging task. Segmentation of retinal blood vessels becomes more difficult in abnormal images with the presence of diseases like hypertension, diabetes, stroke and other vascular disorders. In this work, a new fast framework for automatic retinal blood vessels extraction and denoising has been proposed. Green channel due to its prominent vessel structure is used as an input to morphological filters to eradicate low frequency noise or geometrical entities, *e.g.*, macula, optic disk and other abnormalities. The Generalized Linear Model (GLM) regression is used for non-uniform contrast enhancement followed by Frangi filter for vasculature based enhancement. Masking operation has performed to extract Region of Interest (ROI) for application of moment-preserving thresholding to separate vessel and background pixels. Finally, postprocessing steps are applied to eliminate unconnected pixels and to obtain final binary image. This technique has been validated on the DRIVE and the STARE databases and contested with other competing techniques. Experimental results indicate that the proposed vessel extraction framework outperforms many recent existing methods published in literature.

Keywords: DRIVE, denoising, thresholding, retinal Images, STARE, vessel segmentation

1. INTRODUCTION

The retinal blood vessel dissection is deliberated as a prerequisite in many medical applications related to eye disorders diagnoses and surgery planning. It can be applied for analysis of numerous eye abnormalities such as glaucoma [1], Diabetic Retinopathy (DR) [2, 3] and hypertension [4], *etc.* Moreover, it can be also utilized for examination of vessel features such as vessel width and tortuosity. Retinal abnormalities that change the vascular tree caused visual impairment. Detection of such abnormalities at the primary stage can restrain the blindness to a great extent. Hence, retinal blood vessel extraction and further investigation of its features help in diagnosis of retinal diseases [5]. Retinal vascular manual extraction is very hard and time taken task that needs expertise. Therefore, the evolution of automatic techniques for vessel extraction and vessel width computation is required [6].

Nowadays, digital ophthalmoscopes make it easier to acquire retina digital images. This helps the medical doctors to perform retina vasculature analysis of their patients and

Received June 10, 2016; revised August 12, 2016; accepted October 8, 2016.
Communicated by Jing-Ming Guo.

make it possible to develop automated image investigation techniques. Various methodologies have already been published for retinal vasculature extraction. However, automatic extraction of retinal vessel map is still challenging because of its different structure complications and impact from other sources. The complexities originate due to vessel contrast variations, pattern and orientations; disorders due to the existence of noise and abnormalities of the structures such as lesions, exudates, microaneurysms and other diseased segments. These difficulties might misguide an automatic vessel segmentation method by falsify background to vessels and neglecting the thin vessels [6].

In current work, we presented an automatic approach for retinal vascular tree extraction. This method performs detection of retinal blood vessels through a sequence of applications consist of preprocessing steps for denoising and contrast enhancement (green channel extraction, morphological filters, GLM training, Frangi filter and masking), moment-preserving thresholding for sorting of vessel and background pixels and postprocessing steps to remove unconnected pixels and to obtain final binary image. The later sections discuss the literature review of the existing retinal vessel detection methods, the proposed methodology, the results of experiments and the conclusion.

2. REVIEW OF RETINAL VESSEL SEGMENTATION METHODS

Fraz *et al.* [6] reviewed many retinal vessel detection methods already published. Existing methodologies can be sorted into supervised and unsupervised techniques. Supervised techniques used classifier, trained on manually labeled images by experts from the STARE and the DRIVE datasets to categorized vessel and background pixels while unsupervised techniques didn't require any priori pixel labeling knowledge.

The vessel tracking system depends on the coherence property of veins that trace every vessel from the beginning point. Li *et al.* [7] described the vessel tracking methodology to distinguish every vessel and give more noteworthy vessel details than the pixel based strategies. A novel method utilizing multi-scale line-tracing process and morphological filtering was presented by Vlachos [8]. Matched filter detect the linear segment of retinal vessel network using kernel and Gaussian functions [9]. Numerous advancement have been achieved on Matched Filtering (MF) methods, consisting utilization of global or local thresholding systems [10, 11]. Odstrcilik *et al.* [12] suggested MF and minimum error thresholding based framework to segment retinal vascular network. An innovative vessel detection approach using combination of MF with multi wavelet kernels was introduced by Wang *et al.* [13]. This method used adaptive thresholding and did not need any prior training. Morphological approaches consist of two fundamental steps dilation and erosion. Morphological methods are suitable for investigating shapes in the images which are helpful in detection of retinal vessels [9]. Mendonca *et al.* [14] used combination of mathematical morphology and MF for centerline detection. Martinez *et al.* [2] presented a multi-scale feature extraction approach to extract vessel network. Morphological Component Analysis (MCA) based approach has been proposed for extraction of retinal vessels [15]. Azzopardi *et al.* [16], employed a scheme depend on the Combination Of Shifted Filter Responses (COSFIRE) with competing results which was further improved by Strisciuglio *et al.* [17], utilizing Generalized Matrix Learning Vector Quantization (GMLVQ) technique. Jiang and Mojon [18], used a verification-based multi-

threshold probing framework to extract retinal vessel network. Bankhead *et al.* [19] introduced a technique for retinal vessel detection utilized a wavelet transform. In model-based approaches, Al-Diri *et al.* [20], introduced a scheme depend on two pairs of contours to perceive every vessel border, while observing vessel thickness. Lam *et al.* [21] suggested a framework using regularization based multi-concavity modeling. Espona *et al.* [22] presented a vessel detection technique depend on classical snake algorithm. A new inpainting filter, called Neighborhood Estimator Before Filling (NEBF), and multiple-scale hessian approach has been used for vessel extraction [23]. Mapayi *et al.* [24] presented local adaptive thresholding technique for retinal vessel extraction using Gray Level Cooccurrence Matrix (GLCM) energy information. Graph cut approach has been introduced by Zhao *et al.* [25], for retinal vessel extraction. Asad *et al.* [26] used an ant colony system based scheme for detection of retinal vascular map.

Supervised technique presented by Niemeijer *et al.* [27] used combination of a feature array and the Gaussian MF responses. Then, the *k*-Nearest Neighbor (*kNN*) scheme was applied to project the probability map and thresholding was utilized to detect retinal vessel structure. Staal *et al.* [3] suggested a technique to create a feature array for every pixel utilizing the patch characteristics and the line properties as inputs to the *kNN* classifier. In [28], a radial projection detects the vessel centerlines and the semi-supervised classifier extracts major vessel map. 2-D Gabor wavelet was used by Soares *et al.* [29], for extraction of retinal vasculature. A framework depend on neural networks was presented in [30]. Ricci and Perfetti [31] presented a technique depend on line operators and SVM classifier for pixel sorting. Fraz *et al.* [32] utilized an ensemble of bagged decision trees and a feature array for retinal vessel detection. Tang *et al.* [33] presented a supervised technique for retinal vascular extraction based on SVM and Gabor filter.

3. METHODOLOGY

This section explains the major processing steps of the proposed framework.

3.1 Overview

In this paper, the green band of RGB fundus photograph is utilized as an input for further processing and segmentation. Morphological filters are used on an input image to eliminate low frequency noise and other disease abnormalities. GLM regression is used to learn feature vector for nonlinear contrast enhancement. Feature vector increase the intensity of vessel like pixels and suppress the background pixels, followed by Frangi filter for vasculature based enhancement. Masking extracts the ROI for application of moment-preserving thresholding to segregate vessel and background pixels. At the end, postprocessing steps are utilized to discard the isolated pixels and to acquire the final binary image. Fig. 1 represents the flowchart of the proposed framework with major processing steps.

3.2 Preprocessing Steps

The preprocessing steps used for denoising and contrast enhancement consist of green channel extraction, morphological filters, GLM regression based contrast enhance-

ment, Frangi filter and masking. Green band of color fundus image is used due to its prominent contrast of vessels from background. Morphological top-hat transformation adapted from [14], has been used by introducing two new steps: a closing operator followed by the opening, without using any minimum operator and comparison.

The top-hat operator of an image I with Structuring Element (SE) S_o is as follows

$$T_{open} = I \circ S_o \tag{1}$$

The closing top-hat operator of an image I with structuring element S_c is as follows

$$T_{close} = I \cdot S_c \tag{2}$$

An improved version of top-hat transform modified from [14], is as follows

$$TopHat = I - (I \cdot S_c) \circ S_o \tag{3}$$

Eq. (3), shows our improved top-hat transform, in which I is the input green band photograph while S_c and S_o denote the SEs for closing ($\cdot$) and opening ($\circ$) operators, correspondingly. In this paper, we utilize disk type SEs for both opening and closing operator having radius 8 pixels.

Morphological filters remove geometrical objects such as macula, optic disk and other disease abnormalities before application of GLM regression. Only one time manually segmented image is used for GLM training to learn feature array for contrast enhancement of the vessel like pixels and suppressing background pixels. A Random component, Systematic component and Link function are the three major components of any GLM. A random component describes the probability distribution of response variable X; a systematic component indicates explanatory variables used in a linear predictor function; and a link function refers the link between random and systematic component [34].

The Probability Mass Function (PMF) for the possible outcomes x for variable X is

$$p(x) = \binom{n}{x} \pi^x (1-\pi)^{n-x} \tag{4}$$

where $x = 0, 1, 2, \ldots, n$. This is the special case of the binomial for $n = 1$. The PMF is

$$f(x;\pi) = \pi^x (1-\pi)^{1-x} = (1-\pi)\left[\frac{\pi}{1-\pi}\right]^x = (1-\pi)\exp\left(x \log \frac{\pi}{1-\pi}\right) \tag{5}$$

For x=0 and 1. π is a constant value. The natural parameter $\log \frac{\pi}{1-\pi}$ is the log odds of response 1, the logit of π. GLMs using the logit link are often called logit models. GLM regression based transformation step is applied in place of histogram equalization. It tried to suppress the intensity of non-vessel pixels and increase the contrast of vessel pixels. Further, Frangi filter is applied to perform vasculature based enhancement. Contrast enhancement or similar other techniques perform enhancement in the uniform manner depending on pixel intensity, which can also enhance background noise along with vasculature enhancement in contrast to Frangi filter.

Frangi *et al.* [35], for continuous 2D image $I(\hat{y})$, vascular contrast improvement operator for high intensity vessels is considered as a filter with its response

$$r(\hat{y},\sigma,\beta_1,\beta_2)=\begin{cases}0 & \text{if } \lambda_2(\hat{y},\sigma)>0\\ \exp\left(\dfrac{-\mathcal{R}_{\beta^2}(\hat{y},\sigma)}{2\beta_1^2}\right)\left(1-\exp\left(-\dfrac{S^2(\hat{y},\sigma)}{2\beta_2^2}\right)\right)\end{cases} \tag{6}$$

where $\lambda_1(\hat{y}, \sigma)$ and $\lambda_2(\hat{y}, \sigma)$ are the eigenvalues of the local hessian estimated at $\hat{y}$ at scale σ, such that $|\lambda_1(\hat{y}, \sigma)| < |\lambda_2(\hat{y}, \sigma)|$. The elongated strength $\mathcal{R}_\beta(\hat{y},\sigma)=\dfrac{\lambda_1(\hat{y},\sigma)}{\lambda_2(\hat{y},\sigma)}$ computes the variation from a blob by considering for the eccentricity of the second order ellipse. $\mathcal{R}_\beta(\hat{y}, \sigma)$ cannot differentiate between a line and a boundary. The structureness measure $S(\hat{y}, \sigma) = \sqrt{\lambda_1^2(\hat{y},\sigma)+\lambda_2^2(\hat{y},\sigma)}$ is the norm of the hessian and is calculated to differentiate between vessel and background pixels. The metrics β_1 and β_2 tune the sensitivity of the filter to deviations in $\mathcal{R}_\beta(\hat{y}, \sigma)$ and $S(\hat{y}, \sigma)$ [36]. Frangi filter perform vasculature based enhancement by eliminating unwanted regions. Further, mask is applied to extract ROI. Red channel of RGB retinal input image is used to extract mask due to its prominent contrast between ROI and background. Masking is applied to suppress exterior ROI noise pixels which may appear as vessel pixels.

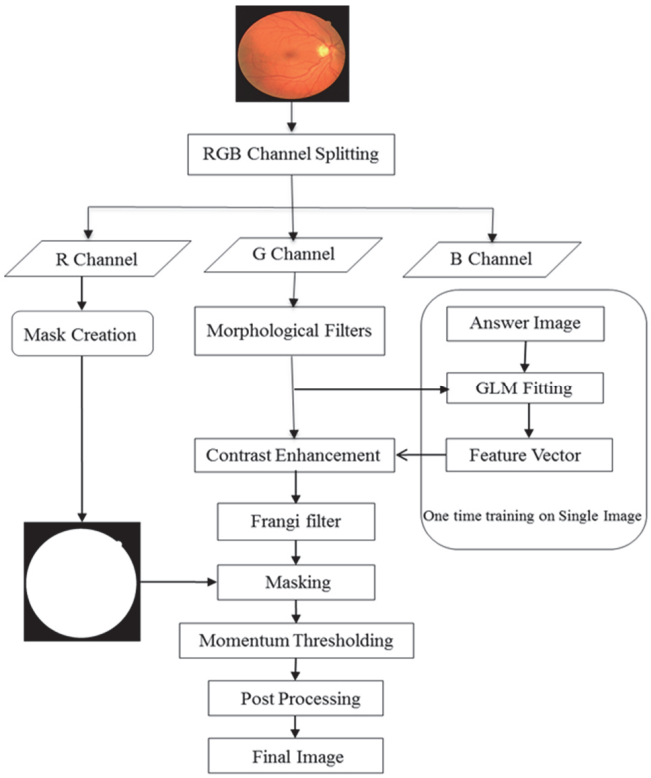

Fig. 1. Flowchart of the proposed framework.

3.3 Moment-Preserving Thresholding

The moment-preserving thresholding by Tsai [37] is used on the ROI of an input image to classify pixels into vessel and background. It found the threshold so that the first three moments of the input photograph are preserved in the output photograph. Input image "*I*" is threshold into two clusters, the below and the above-threshold pixels. For image "*I*" with *n* number of pixels whose pixel intensity is $I(k, 1)$ at pixel (k, l) and the ith moment m_i of *I* is defined as

$$m_i = \left(\frac{1}{n}\right)\sum_k \sum_l I^i(k,l), \qquad i = 1,\ 2,\ 3,\ \ldots \tag{7}$$

Histogram of *I* can also be used to calculate moments as follows

$$m_i = \left(\frac{1}{n}\right)\sum_j n_j (z_j)^i \sum_j p_j (z_j)^i \tag{8}$$

where n_j is the total number of pixels in *I* with pixel intensity value z_j and $p_j = \frac{n_j}{n}$. Bi-level image pixels consists of two pixel intensity values z_0 and z_1 where $z_0 < z_1$. The moment-preserving method select such a threshold that if all below-threshold pixel intensity values denoted by p_0 in *I* are substituted by z_0 and all above-threshold pixel intensity values denoted by p_1, substituted by z_1, then the first three moments of image *I* are preserved in the output binary image *g* which is an ideal unblurred version of *I*. The resulting image consist of two groups vessel and background pixels. The first three moments of an image *g* are

$$m_i' = \sum_{j=0}^{1} p_j (z_j)^i, \qquad i = 1,\ 2,\ 3. \tag{9}$$

And preserving the first three moments in *g* means the following equalities:

$$m_i' = m_i, \qquad i = 1, 2, 3, \tag{10}$$

where

$$p_0 + p_1 = 1. \tag{11}$$

The four equalities described by Eqs. (10) and (11) above are equivalent to

$$\begin{aligned} p_0 z_0^0 + p_1 z_1^0 &= m_0 \\ p_0 z_0^1 + p_1 z_1^1 &= m_1 \\ p_0 z_0^2 + p_1 z_1^2 &= m_2 \\ p_0 z_0^3 + p_1 z_1^3 &= m_3 \end{aligned} \tag{12}$$

where m_i with $i = 1, 2, 3$ are computed by Eq. (7) or Eq. (8) and $m_0 = 1$.

3.4 Postprocessing Steps

The resultant image of moment-preserving thresholding is further postprocessed to remove unconnected pixels. The output consequences generally comprise of some small isolated segments due to noise and these segments are sometimes erroneously noticed as the vessels. Based on the relationship with the retinal vessels, we eradicate less than or equal to fifty isolated pixels considered as a background or a part of the background noise. Figs. 2 and 3, represents visual inspection of the major processing steps of the proposed system using the DRIVE [38] and the STARE [10] databases, respectively.

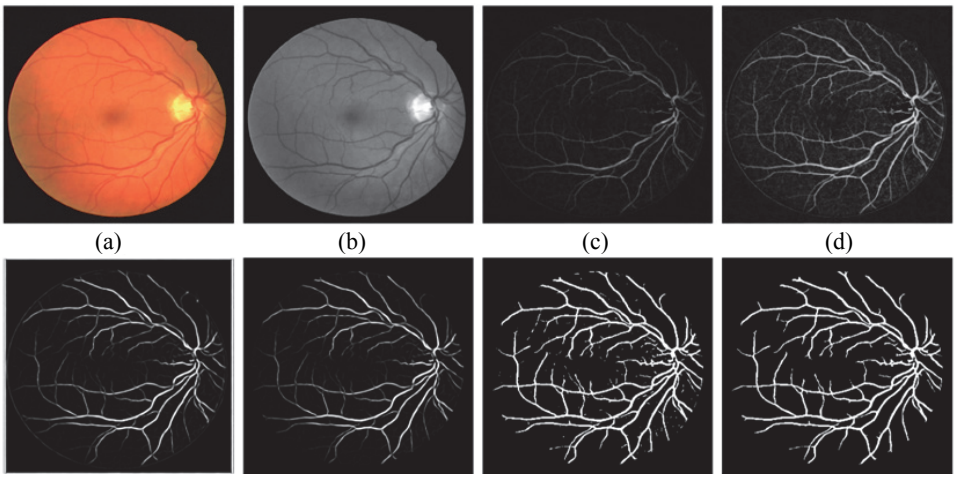

Fig. 2. (a) DRIVE dataset color photograph; (b) Green channel; (c) Morphological filters resultant image; (d) GLM contrast enhanced image; (e) Frangi filter's image; (f) Masking; (g) moment-preserving thresholding output; (h) Postprocessed final image.

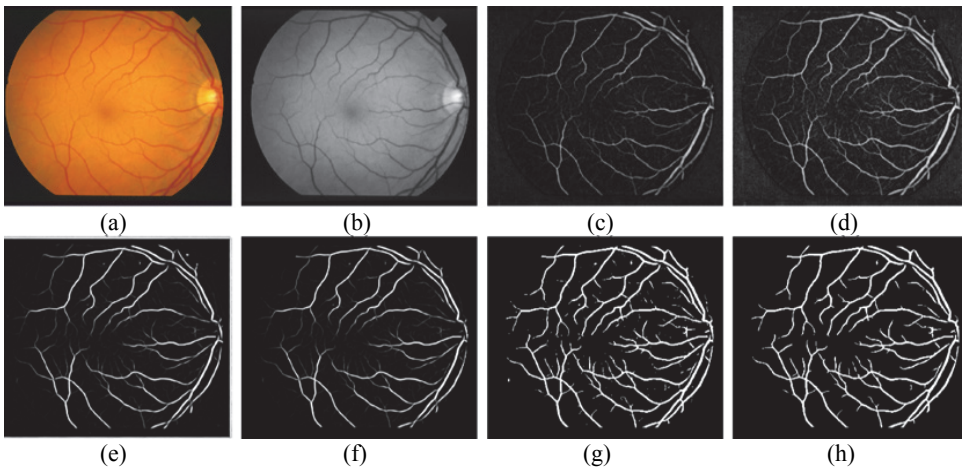

Fig. 3. (a) STARE dataset RGB retinal image; (b) Green channel; (c) Morphological filters resultant photograph; (d) GLM contrast enhanced output; (e) Frangi filter's photograph; (f) Masking; (g) Moment-preserving thresholding output; (h) Postprocessed final image.

4. EXPERIMENTAL VALIDATION AND ANALYSIS

The proposed framework has been verified on the DRIVE and the STARE databases and contested with other competing methods. Both datasets consist of second human observer's images of vessels for the comparative efficiency assessment of various vessel extraction techniques. The DRIVE dataset consist of 40 images: 33 healthy retina images and 7 abnormal photographs. The dataset is distributed into two sets a test set and a training set, each comprising 20 photographs. These photographs were captured from Canon CR5 non-mydriatic 3CCD camera with a 45 degree Field Of View (FOV). The acquired photographs consist 8 bits per color plane at 768×584 resolution. The ratio of positive to negative samples is 0.17. The STARE dataset consists of 20 retinal photographs and out of 20 photographs there are 10 normal retinal images and the residual belongs to abnormal retinal photographs. These photographs were acquired by a TopCon TRV-50 fundus camera at 35 degree FOV. The acquired photographs comprise 8 bits per color channel at 605×700 pixels. The ratio of positive to negative samples is 0.11. Experiments were performed using MATLAB 2013a.

The commonly used performance measures are Accuracy (Acc), Sensitivity (Sn) and Specificity (Sp). Sensitivity shows the strength of a delineation method to segment the vessel pixels while specificity describes the strength of a delineation method to extract non-vessel pixels. The accuracy is extent of distinguished vessel pixels which are genuine vessel pixels. This can be defined as follows

$$Acc = \frac{TP + TN}{TP + FP + TN + FN}, \tag{13}$$

$$Sn = \frac{TP}{TP + FN}, \tag{14}$$

$$Sp = \frac{TN}{TN + FP}, \tag{15}$$

where TP, TN, FP and FN denotes the True Positive which are rightly detected as a vessel pixel, True Negative which are rightly segmented as a background pixels, False Positive in which background pixels are considered as a vessel pixels, and False Negative when vessel pixels are extracted as a non-vessel pixels respectively.

We have compared the proposed GLM technique for contrast enhancement with the CLAHE generally used for contrast enhancement in the literature. The final visual results both with GLM and CLAHE method are depicted in the Fig. 4, while the quantitative results on the DRIVE database are tabulated in Table 1. The effect on the consequences of masking used in the proposed approach to excerpt ROI is also shown in Table 1. The pictorial representation of mask application is demonstrated in Fig. 5. Table 1 indicates that proposed GLM scheme produced better results than CLAHE and also computational efficient than CLAHE. The GLM performs training only one time in 0.1507 seconds. The visual results also indicate the better efficiency of GLM and the mask application.

Table 1. Evaluation of GLM, CLAHE and masking tools for retinal vessel extraction.

Images	Proposed GLM				CLAHE			
	Acc	*Sn*	*Sp*	Time	*Acc*	*Sn*	*Sp*	Time
1	0.9659	0.8186	0.9824	0.0271	0.9594	0.8117	0.9704	0.0975
2	0.9623	0.8241	0.9734	0.0255	0.9495	0.8092	0.9552	0.1389
3	0.9654	0.8083	0.9787	0.0280	0.9602	0.7962	0.9640	0.1053
	Proposed Masking				Without Masking			
1	0.9674	0.8188	0.9806		0.9163	0.6956	0.9359	
2	0.9651	0.8303	0.9755		0.9188	0.7182	0.9344	
3	0.9642	0.7925	0.9802		0.9129	0.7354	0.9294	

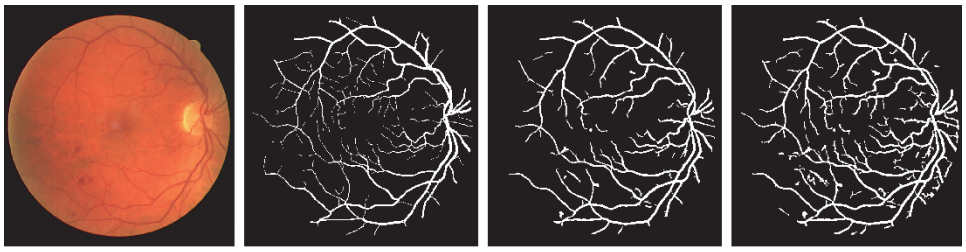

(a) (b) (c) (d)

Fig. 4. (a) Color retinal photograph; (b) Manually labelled photograph; (c) Proposed system final result using GLM approach; (d) Proposed method final image using CLAHE.

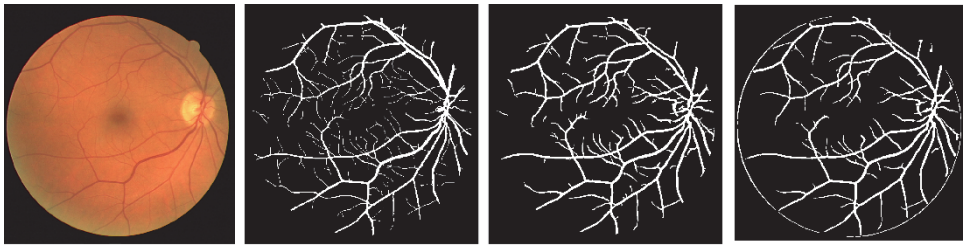

(a) (b) (c) (d)

Fig. 5. (a) Color retinal photograph; (b) Manually labelled photograph; (c) Proposed system final result with application of Mask; (d) Final image without application of Mask.

We have computed the *Acc*, *Sn* and *Sp* for both the DRIVE and the STARE datasets. Table 2 represents that the proposed system reached a highest accuracy than all other paralleled techniques on the DRIVE database, while in the case of STARE dataset supervised methods Staal [3], Ricci [31] and Fraz [32] have 0.01, 0.013 and 0.002 greater accuracy than proposed method. On the STARE dataset, unsupervised methods Wang [13], Imani [15], Strisciuglio [17] and Annunziata [23] showed a slightly higher accuracy than a proposed method. The results of Vlachos [8], Odstrcilik [12], Wang [13], Imani [15], Azzopardi [16], Strisciuglio [17], Espona [22], Annunziata [23], Mapayi [24], Zhao [25], Asad [26], Niemeijer [27], Marin [30], Ricci [31] and Fraz [32] are extracted from their published articles while Staal [3] and Soares [29] are retrieved from their websites

using the segmented images. Both publically available datasets consist of manually labelled photographs, which are added in the evaluation. In Table 2, we have displayed the results obtained by the proposed technique on the DRIVE and the STARE datasets contrasted with others segmentation techniques published in literature. The assessment results of the proposed system on the DRIVE and the STARE databases are superior to many of other techniques and affirm the adequacy of the proposed strategy. Figs. 6 and 7, represent visual results of the proposed vessel extraction framework utilizing normal photographs of the DRIVE and the STARE databases, correspondingly.

Table 2. Performance assessment of various methods for retinal vessel extraction.

Methodology	Year	DRIVE			STARE		
		Acc	*Sn*	*Sp*	*Acc*	*Sn*	*Sp*
Unsupervised							
Human observer		0.947	0.776	0.972	0.935	0.895	0.939
Vlachos [8]	2010	0.929	0.747	0.955	–	–	–
Odstrcilik [12]	2013	0.934	0.706	0.969	0.934	0.785	0.951
Wang [13]	2013	0.946	–	–	0.952	–	–
Imani [15]	2015	0.952	0.752	0.975	0.959	0.750	0.975
Azzopardi [16]	2015	0.944	0.765	0.970	0.949	0.772	0.970
Strisciuglio [17]	2015	0.947	0.773	0.972	0.954	0.801	0.972
Espona [22]	2007	0.932	0.663	0.968	–	–	–
Annunziata [23]	2015	–	–	–	0.956	0.713	0.984
Mapayi [24]	2015	0.951	0.765	0.963	0.951	0.764	0.965
Zhao [25]	2015	0.953	0.744	0.978	0.951	0.786	0.975
Asad [26]	2016	–	–	–	0.934	0.748	0.954
Proposed	2016	**0.960**	0.747	0.980	0.951	0.778	0.966
Supervised							
Niemeijer [27]	2004	0.942	0.714	–	–	–	–
Staal [3]	2004	0.944	0.719	0.977	0.961	0.697	0.981
Soares [29]	2005	0.946	0.723	0.976	0.948	0.720	0.974
Ricci [31]	2007	0.959	–	–	**0.964**	–	–
Marin [30]	2011	0.945	0.705	0.980	0.952	0.694	0.981
Fraz [32]	2012	0.948	0.741	0.981	0.953	0.755	0.976
Tang [33]	2015	0.950	–	–	–	–	–

"–" shows that data is not available

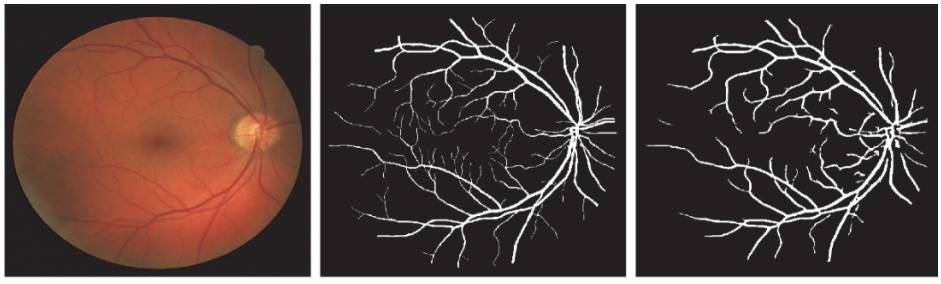

(a) (b) (c)

Fig. 6. (a) RGB normal retinal image from DRIVE dataset; (b) Manual segmented image by a human observer; (c) Proposed method final binary image.

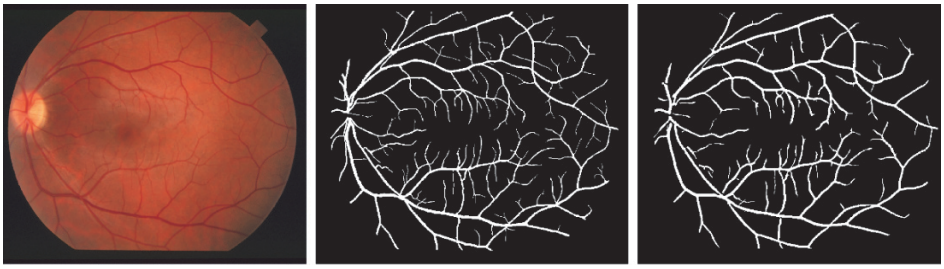

(a) (b) (c)

Fig. 7. (a) RGB normal retinal image from STARE dataset; (b) Manual segmented image by a human observer; (c) Proposed method final binary image.

For pathological cases, the effectiveness of the proposed system has been validated by comparing the results of various techniques on the both datasets, displayed in Table 3. The tabulated statistics clearly indicates that the proposed technique outperforms many other vessel extraction methods reported in literature for abnormal cases. It obtained superior performance than Mendonca & Campilho [14] Hoover *et al.* [10] while Annunziata *et al.* [23] performs slightly better results than ours. Soares *et al.* [29] result is nearby to the proposed method. Figs. 8 and 9 represent pictorial inspection for pathological photographs of the DRIVE and the STARE databases, respectively.

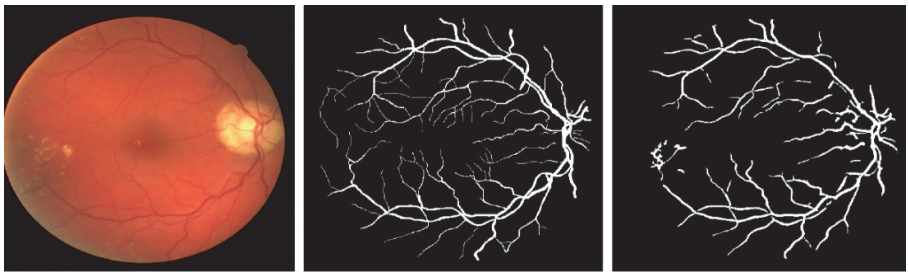

(a) (b) (c)

Fig. 8. (a) DRIVE dataset RGB abnormal retinal image; (b) Manual segmented image by a human observer; (c) Proposed method final binary image.

(a) (b) (c)

Fig. 9. (a) STARE dataset RGB abnormal retinal image; (b) Manual segmented image by a human observer; (c) Proposed method final binary image.

In addition, the performance of proposed technique has been also judged in term of AUC. An ROC curve is a pictorial representation of sensitivity versus false positive fractions (1−*Sp*). The nearer the curve reaches to the top left corner, the better is the performance of the framework. AUC is the mainly utilized performance parameter from the ROC curve, which is 1 for an ideal scheme. Fig. 10 shows ROC curves for the DRIVE and the STARE databases. The AUC of the proposed framework has been contested with other existing techniques as exposed in Table 4. The proposed scheme showed higher AUC results than the other vessel extraction methods published in literature on the both databases.

Table 3. Accuracy comparison with different methods on abnormal retinal cases.

Image Type	Method	Year	Acc
Abnormal	Human observer		0.9425
	Annunziata [23]	2015	**0.9565**
	Mendonca [14]	2006	0.9388
	Hoover [10]	2000	0.9211
	Soares [29]	2005	0.9416
	Proposed	2016	0.9401

Table 4. AUC results of proposed method compared with various methods.

Technique	Year	AUC (DRIVE)	AUC (STARE)
Human observer		0.874	0.917
Malek [11]	2013	0.924	0.934
Odstrcilik [12]	2013	0.9519	0.9569
Imani [15]	2015	0.9544	0.9526
Azzopardi [16]	2015	0.9614	0.9563
Strisciuglio [17]	2015	0.9588	0.9629
Lam [21]	2010	0.9614	0.9739
Annunziata [23]	2015	not available	0.9655
Mapayi [24]	2015	0.9658	0.9781
Zhao [25]	2015	0.861	0.881
Marin [30]	2011	0.9588	**0.9769**
Ricci [31]	2007	0.9633	0.9680
Fraz [32]	2012	**0.9747**	0.9768
Tang [33]	2015	0.9620	not available
Proposed	2016	0.9658	0.9751

Processing time assessment of different retinal vessel identification techniques is revealed in Table 5. The proposed system is computationally very fast than many other recent published techniques. We included only those methods in comparison whose hardware are same or advanced than ours. Supervised methods take a long computation time as compared to unsupervised methods. For example, Soares [29] requires nine hours for training and then three more minutes for processing. The proposed framework is unsupervised and requires less computation time.

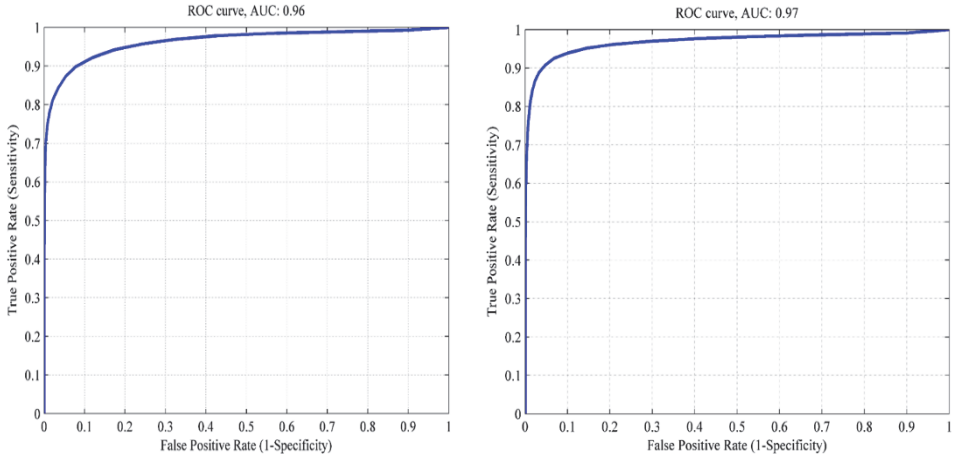

Fig. 10. ROC curve of proposed framework for normal image of the DRIVE dataset (left) and STARE dataset (right).

Table 5. Processing time comparison.

Method	Year	Processing Time	Computer Specifications	Software
Proposed	2016	6.1 Sec	Core i3 CPU, 2.53 GHz, 4 GB RAM.	MATLAB
Bankhead [19]	2012	22.45 Sec		MATLAB
Azzopardi [16]	2015	11.83 Sec		MATLAB
Dai [39]	2015	1 min 46 Sec		MATLAB
Vlachos [8]	2010	9.3 Sec		MATLAB
Mapayi [24]	2015	1.9 to 2.6 Sec	Intel Core i5 2410M CPU, 2.30GHz, 4GB RAM.	MATLAB
Zhao [25]	2015	4.6 Sec	HP Intel Core i3 CPU, 3.1 GHz, 8 GB RAM	MATLAB & C++
Asad [26]	2016	2 mins and 45 Sec	Intel Core i3 CPU, 2.53 GHz, 3 GB RAM	MATLAB

5. CONCLUSIONS

In this article, we proposed a fast and accurate methodology for retinal vessels extraction and denoising based on GLM and moment-preserving thresholding. It has been shown that proposed framework produced good visual results. The proposed framework performance has been assessed by utilizing openly accessible datasets: DRIVE and STARE. It has been exposed that proposed method obtained higher accuracy, sensitivity, specificity and AUC values when compared to the results of various recent methods. Experimental results validated that the proposed framework can detect both wide and thin retinal vessels precisely of the DRIVE and the STARE datasets. It has also been validated that the contrast is prominently enhanced by GLM and make it convenient to eradicate noise and extract blood vessels. In addition, the proposed scheme also requires less computation time on both databases.

REFERENCES

1. H. Leung, J. J. Wang, E. Rochtchina, T. Y. Wong, R. Klein, and P. Mitchell, "Impact of current and past blood pressure on retinal arteriolar diameter in an older population," *Journal of Hypertension*, Vol. 22, 2004, pp. 1543-1549.
2. M. E. Martinez-Perez, A. D. Hughes, S. A. Thom, A. A. Bharath, and K. H. Parker, "Segmentation of blood vessels from red-free and fluorescein retinal images," *Medical Image Analysis*, Vol. 11, 2007, pp. 47-61.
3. J. Staal, M. D. Abràmoff, M. Niemeijer, M. A. Viergever, and B. van Ginneken, "Ridge-based vessel segmentation in color images of the retina," *IEEE Transactions on Medical Imaging*, Vol. 23, 2004, pp. 501-509.
4. P. Mitchell, H. Leung, J.J. Wang, E. Rochtchina, A. J. Lee, T. Y. Wong, and R. Klein, "Retinal vessel diameter and open-angle glaucoma: the blue mountains eye study," *Ophthalmology*, Vol. 112, 2005, pp. 245-250.
5. J. J. Kanski, *Clinical Ophthalmology*, 6th ed., Elsevier Health Sciences, London, UK, 2007.
6. M. M. Fraz, P. Remagnino, A. Hoppe, B. Uyyanonvara, A. R. Rudnicka, C. G. Owen, and S. A. Barman, "Blood vessel segmentation methodologies in retinal images – a survey," *Computer Methods and Programs in Biomedicine*, Vol. 108, 2012, pp. 407-433.
7. H. Li, J. Zhang, Q. Nie, and L. Cheng, "A retinal vessel tracking method based on bayesian theory," in *Proceedings of the 8th IEEE Conference on Industrial Electronics and Applications*, 2013, pp. 232-235.
8. M. Vlachos and E. Dermatas, "Multi-scale retinal vessel segmentation using line tracking," *Computerized Medical Imaging and Graphics*, Vol. 34, 2010, pp. 213-227.
9. N. Patton, T. M. Aslam, T. MacGillivray, I. J. Deary, B. Dhillon, R. H. Eikelboom, K. Yogesan, and I. J. Constable, "Retinal image analysis: concepts, applications and potential," *Progress in Retinal and Eye Research*, Vol. 25, 2006, pp. 99-127.
10. A. Hoover, V. Kouznetsova, and M. Goldbaum, "Locating blood vessels in retinal images by piecewise threshold probing of a matched filter response," *IEEE Transactions on Medical Imaging*, Vol. 19, 2000, pp. 203-210.
11. J. Malek and R. Tourki, "Blood vessels extraction and classification into arteries and veins in retinal images," in *Proceedings of the 10th IEEE International Multi-Conference on Systems*, *Signals and Devices*, 2013, pp. 1-6.
12. J. Odstrcilik, R. Kolar, A. Budai, J. Hornegger, J. Jan, J. Gazarek, T. Kubena, P. Cernosek, O. Svoboda, and E. Angelopoulou, "Retinal vessel segmentation by improved matched filtering: evaluation on a new high-resolution fundus image database," *Image Processing*, IET, Vol. 7, 2013, pp. 373-383.
13. Y. Wang, G. Ji, P. Lin, and E. Trucco, "Retinal vessel segmentation using multiwavelet kernels and multiscale hierarchical decomposition," *Pattern Recognition*, Vol. 46, 2013, pp. 2117-2133.
14. A. M. Mendonca and A. Campilho, "Segmentation of retinal blood vessels by combining the detection of centerlines and morphological reconstruction," *IEEE Transactions on Medical Imaging*, Vol. 25, 2006, pp. 1200-1213.

15. E. Imani, M. Javidi, and H. R. Pourreza, "Improvement of retinal blood vessel detection using morphological component analysis," *Computer Methods and Programs in Biomedicine*, Vol. 118, 2015, pp. 263-279.
16. G. Azzopardi, N. Strisciuglio, M. Vento, and N. Petkov, "Trainable COSFIRE filters for vessel delineation with application to retinal images," *Medical Image Analysis*, Vol. 19, 2015, pp. 46-57.
17. N. Strisciuglio, G. Azzopardi, M. Vento, and N. Petkov, "Multiscale blood vessel delineation using B-COSFIRE filters," *Computer Analysis of Images and Patterns*, Springer, 2015, pp. 300-312.
18. X. Jiang and D. Mojon, "Adaptive local thresholding by verification-based multithreshold probing with application to vessel detection in retinal images," *IEEE Transactions on Pattern Analysis and Machine Intelligence*, Vol. 25, 2003, pp. 131-137.
19. P. Bankhead, C. N. Scholfield, J. G. McGeown, and T. M. Curtis, "Fast retinal vessel detection and measurement using wavelets and edge location refinement," *PloS One*, Vol. 7, 2012, p. e32435.
20. B. Al-Diri, A. Hunter, and D. Steel, "An active contour model for segmenting and measuring retinal vessels," *IEEE Transactions on Medical Imaging*, Vol. 28, 2009, pp. 1488-1497.
21. B. S. Lam, Y. Gao, and A. W. C. Liew, "General retinal vessel segmentation using regularization-based multiconcavity modeling," *IEEE Transactions on Medical Imaging*, Vol. 29, 2010, pp. 1369-1381.
22. L. Espona, M. J. Carreira, M. Ortega, and M. G. Penedo, "A snake for retinal vessel segmentation," in *Proceedings of the 3rd Iberian Conference on Pattern Recognition and Image Analysis*, LNCS 4478, 2007, pp. 178-185.
23. R. Annunziata, A. Garzelli, L. Ballerini, A. Mecocci, and E. Trucco, "Leveraging multiscale hessian-based enhancement with a novel exudate inpainting technique for retinal vessel segmentation," *IEEE Journal of Biomedical and Health Informatics*, Vol. 20, 2016, pp. 1129-1138.
24. T. Mapayi, S. Viriri, and J. R. Tapamo, "Adaptive thresholding technique for retinal vessel segmentation based on GLCM-energy information," *Computational and Mathematical Methods in Medicine*, 2015.
25. Y. Zhao, Y. Liu, X. Wu, S. P. Harding, and Y. Zheng, "Retinal vessel-segmentation: An efficient graph cut approach with retinex and local phase," *PloS One*, Vol. 10, 2015, p. e0122332.
26. A. H. Asad and A. E. Hassaanien, "Retinal blood vessels segmentation based on bio-inspired algorithm," *Applications of Intelligent Optimization in Biology and Medicine*, Vol. 96, 2016, pp. 181-215.
27. M. Niemeijer, J. Staal, B. van Ginneken, M. Loog, and M. D. Abramoff, "Comparative study of retinal vessel segmentation methods on a new publicly available database," *Medical Imaging*, Vol. 5370, 2004, pp. 648-656.
28. X. You, Q. Peng, Y. Yuan, Y. M. Cheung, and J. Lei, "Segmentation of retinal blood vessels using the radial projection and semi-supervised approach," *Pattern Recognition*, Vol. 44, 2011, pp. 2314-2324.
29. J. V. Soares, J. J. Leandro, R. M. Cesar-Jr, H. F. Jelinek, and M. J. Cree, "Using the 2-D morlet wavelet with supervised classification for retinal vessel segmentation," in

Proceedings of the 18th Brazil Symposium of Computer Graphics Image Processing, 2005.
30. D. Marín, A. Aquino, M. E. Gegúndez-Arias, and J. M. Bravo, "A new supervised method for blood vessel segmentation in retinal images by using gray-level and moment invariants-based features," *IEEE Transactions on Medical Imaging*, Vol. 30, 2011, pp. 146-158.
31. E. Ricci and R. Perfetti, "Retinal blood vessel segmentation using line operators and support vector classification," *IEEE Transactions on Medical Imaging*, Vol. 26, 2007, pp. 1357-1365.
32. M. M. Fraz, P. Remagnino, A. Hoppe, B. Uyyanonvara, A. R. Rudnicka, C. G. Owen, and S. A. Barman, "An ensemble classification-based approach applied to retinal blood vessel segmentation," *IEEE Transactions on Biomedical Engineering*, Vol. 59, 2012, pp. 2538-2548.
33. S. Tang, T. Lin, J. Yang, J. Fan, D. Ai, and Y. Wang, "Retinal vessel segmentation using supervised classification based on multi-scale vessel filtering and gabor wavelet," *Journal of Medical Imaging and Health Informatics*, Vol. 5, 2015, pp. 1571-1574.
34. A. Agresti and M. Kateri, *Categorical Data Analysis*, Springer Berlin Heidelberg, 2011, pp. 206-208.
35. A. F. Frangi, W. J. Niessen, R. M. Hoogeveen, T. Van Walsum, and M. A. Viergever, "Model-based quantitation of 3-D magnetic resonance angiographic images," *IEEE Transactions on Medical Imaging*, Vol. 18, 1999, pp. 946-956.
36. S. Bouattour and D. Paulus, "Vessel enhancement in 2D angiographic images," *Functional Imaging and Modeling of the Heart*, 2007, pp. 41-49.
37. W. H. Tsai, "Moment-preserving thresholding: A new approach," *Computer Vision*, *Graphics*, *and Image Processing*, Vol. 29, 1985, pp. 377-393.
38. Research Section, Digital Retinal Image for Vessel Extraction (DRIVE) Database, Utrecht, The Netherlands, University Medical Center Utrecht, Image Sciences Institute, http://www.isi.uu.nl/Research/Databases/DRIVE/.
39. P. Dai, H. Luo, H. Sheng, Y. Zhao, L. Li, J. Wu, Y. Zhao, and K. Suzuki, "A new approach to segment both main and peripheral retinal vessels based on gray-voting and Gaussian mixture model," *PloS One*, Vol. 10, 2015, p. e0127748.

Khan Bahadar Khan received the M.S. degree in Electronic Engineering from International Islamic University Islamabad (IIUI), Pakistan. He is currently pursuing the Ph.D. degree in the Department of Electronic Engineering, IIUI, Pakistan. His research interests include medical image processing, signal processing, computer vision and machine learning.

Amir A. Khaliq obtained his Ph.D. in Electronic Engineering from International Islamic University, Pakistan. His research interest is mainly in the field of Wireless Communication, Digital Signal Processing, and Medical Image Processing. He is currently the Chairman and Professor of the Department of Electronic Engineering, International Islamic University, Pakistan. He has published more than 40 papers in various international and national conferences and journals.

Muhammad Shahid obtained his Telecommunication Engineering degree in 2009 in the Department of Telecommunication Engineering, National University of Computer and Emerging Sciences. He completed MS computer engineering in 2016 in the Department of Electrical Engineering at Capital University of Science and Technology Islamabad, Pakistan. His research interests are medical image processing, communication and signal processing.